Bulletin T.CXLVIII de l'Académie serbe des sciences et des arts – 2025
Classe des Sciences mathématiques et naturelles
Sciences mathématiques, № 50

TOMOGRAPHIC APPROACH TO QUARK-GLUON PLASMA: A REVIEW OF THE DREENA FRAMEWORK AND ITS APPLICATIONS

MAGDALENA DJORDJEVIC

(Accepted at the 9th Meeting, held on December 26, 2025)

A b s t r a c t. We present an overview of a theoretical and computational framework designed to extract fundamental properties of the quark-gluon plasma (QGP) created in ultrarelativistic heavy-ion collisions. It is an extended version of my inaugural lecture delivered on 2*nd meeting of Department of Mathematics, Physics and Geosciences in the Serbian Academy of Sciences and Arts under the same title on March* $28, 2025$*. The approach combines dynamical energy loss theory with realistic hydrodynamic backgrounds, enabling quantitative tomography of the QGP. A key emphasis is placed on the synergy between high-p_T and low-p_T observables, supported by the DREENA numerical framework, which allows direct comparison of theoretical predictions with experimental data. This review outlines the motivation, methodology, and major findings of this research direction, providing the foundation for the next generation of precision studies in heavy-ion physics.*

AMS Mathematics Subject Classification (2000): 81V05, 81T28, 76Y05, 65D30.

Key Words: quark-gluon plasma, heavy-ion collisions, QGP tomography, dynamical energy loss, DREENA framework

1. *Introduction*

Quantum Chromodynamics (QCD) predicted that a new form of matter [1, 2], consisting of deconfined and interacting quarks, antiquarks, and gluons, is created at extremely high energy densities. According to current cosmological models, this

new state of matter — known as quark-gluon plasma (QGP) [3, 4, 5, 6] — existed microseconds after the Big Bang [7].

Today, QGP is created in miniature versions of the Big Bang, often termed "Little Bangs," through ultra-relativistic collisions of heavy ions [4, 5]. These collisions produce a rapidly expanding fireball of quarks and gluons, which thermalizes into QGP. As the system cools, and the temperature (T) drops below the critical temperature T_c, quarks and gluons hadronize, transitioning back to confined states.

The primary scientific objective of the RHIC (Relativistic Heavy Ion Collider) at Brookhaven National Laboratory and the heavy-ion program at the Large Hadron Collider (LHC) at CERN is to study this exotic form of matter. Achieving this objective requires an iterative process of theoretical modeling and experimental validation. To date, the formation of QGP at RHIC and LHC has been confirmed through two principal lines of evidence [4, 5, 8]:

- Low transverse momentum (p_T) observables are well described by relativistic hydrodynamics, indicating that the QGP behaves as a nearly perfect fluid (see e.g., [9]).

- High-p_T observables are consistent with predictions from perturbative QCD (pQCD), and show that energetic partons lose energy while traversing the dense QGP medium, signaling strong interaction with an opaque medium [10].

With the QGP formation now established, current research focuses on determining the properties of this extreme state of matter.

2. *QGP as a perfect fluid*

Initial theoretical expectations suggested that QGP would behave like a weakly interacting gas, due to asymptotic freedom and color screening [11]. However, the success of hydrodynamic models in describing soft observables implied instead that QGP behaves as a nearly perfect fluid — a result that was surprising [5].

Notably, these models estimate the shear viscosity to entropy density ratio (η/s) to be close to the conjectured lower bound obtained via the AdS/CFT correspondence [12]. Such perfect fluid behavior is exceptionally rare: even superfluid ^{3}He is not classified as a perfect fluid, and everyday fluids like water exhibit significantly larger η/s. Consequently, systems with such low viscosity are exceedingly uncommon in nature [13].

Interestingly, perfect fluidity has also been observed in ultracold fermionic atomic gases under specific experimental conditions. This suggests intriguing parallels between systems at vastly different temperature scales [13].

3. *Perfect fluid being too perfect*

While the picture of the QGP as a nearly perfect fluid has been highly influential in shaping our understanding of the strongly-coupled regime, it is increasingly recognized as an idealization. In particular, hydrodynamic simulations are often insensitive to the temperature dependence of η/s in the QGP phase. For example, in [14], a model with a tenfold increase in η/s between T_c and $2T_c$ led to negligible changes in RHIC observables and only a modest 10% variation at the LHC.

A similar insensitivity to rising η/s with temperature was found through different modeling techniques [15]. This has led to the notion of the "perfect fluid being too perfect" [15], referring to the idealized picture in describing QGP as a perfect fluid throughout its evolution [15, 16, 17, 18].

Additional support for a more nuanced picture of the QGP medium comes from studies of other substances, which typically exhibit a minimum in η/s near the phase transition, followed by an increase with temperature [19]. In QGP, the temperature varies significantly during its evolution: for instance, at the LHC, T spans roughly from $4T_c$ to T_c, while in the early Universe, the range is even broader. Motivated by this, over the past decade several state-of-the-art Bayesian analyses have been performed, combining hydrodynamic predictions with low-p_T data [20, 16, 21, 22, 23]. However, despite their sophistication, these studies have consistently yielded a weak constraints on bulk QGP properties (e.g., η/s) at higher temperatures.

4. *Why look beyond the soft sector?*

Bulk QGP properties are traditionally extracted from hydrodynamic modeling constrained by low-p_T observables, which reflect the collective evolution of approximately 99.9% of the produced QCD matter. These studies have led to important insights, including the discovery of near-perfect fluidity of the medium.

However, as emphasized above, certain fundamental properties - such as the temperature dependence of the shear viscosity η/s or the early-time thermalization scale - remain poorly constrained when relying solely on low-p_T data and their theoretical interpretations.

This motivates a search for complementary observables that probe the medium from a different perspective. In particular, rare high-p_T partons interact differently with the QGP: they undergo hard, perturbative scatterings and lose energy via medium-induced processes. These high-energy interactions offer a window into QGP structure that is largely orthogonal to the soft sector.

With abundant high-p_T data already available - and more coming from LHC Run 3 and sPHENIX - we now have the precision and coverage required to address deeper structural questions about the medium. The key question is: *can these rare*

probes be used not only to study energy loss mechanisms, but also to constrain the underlying bulk properties of the QGP?

5. *High-p_T observables as tomographic probes*

High-energy partons interact with the QGP via multiple scatterings and radiative processes, leading to substantial energy loss. This energy loss is manifested experimentally as a suppression of high-p_T hadron yields, quantified by the nuclear modification factor R_{AA}, which is considered to be an excellent probe of high-p_T parton-medium interactions [10].

Moreover, in non-central collisions, the overlap region of the colliding nuclei acquires an almond-like shape in the transverse plane, resulting in anisotropic spatial geometry of the QGP. Since high-p_T partons are produced at different positions and propagate in various directions, they traverse path lengths that depend on the azimuthal angle with respect to the reaction plane. As a result, azimuthal asymmetries develop in the high-p_T hadron distributions, quantified by the second harmonic coefficient v_2. This observable is particularly sensitive to the path-length dependence of parton energy loss and, consequently, to the QGP's dynamical evolution [24].

Despite their clear potential, high-p_T observables have been largely underutilized for inferring bulk QGP properties - primarily due to several persistent theoretical and computational challenges, including the use of simplified energy loss models and fixed QGP backgrounds.

Thus, to fully exploit this potential, a theoretical framework is needed that can accurately describe the interactions of high-p_T partons with the QCD medium, while consistently embedding them within arbitrarily evolving background. This need motivates the development of the DREENA framework, introduced in the following section.

6. *Tomographic strategy and the DREENA framework*

To exploit high-p_T observables for QGP tomography, we have developed the DREENA (*Dynamical Radiative and Elastic ENergy loss Approach*) framework. DREENA combines a dynamical, QCD-based energy loss formalism with realistic hydrodynamic temperature profiles, enabling high-precision theoretical predictions across multiple collision energies and centralities.

- A dynamical energy loss formalism derived in a finite-size, finite-temperature QCD medium, with no reliance on static scattering centers (outlined in the next section),
- Full compatibility with arbitrary temperature profiles obtained from state-of-

the-art hydrodynamic simulations,

- Computational efficiency that allows large-scale, event-by-event analyses across multiple collision energies and systems.

This section provides an overview of the goals and structure of the DREENA approach. The next sections will discuss the theoretical foundations and numerical implementation in detail.

7. *Dynamical energy loss formalism as a tool for QGP tomography*

To use high-$p_\perp$ observables as a QGP tomographic probe, it is essential to employ a realistic and well-founded theoretical description of parton energy loss in the medium. In our approach, we utilize the dynamical energy loss formalism, which incorporates several key physical ingredients that make it particularly well suited for this purpose:

1. **Finite-size and finite-temperature QGP with dynamical constituents:** The formalism is based on thermal QCD field theory at finite temperature and volume [25, 26], and treats QGP constituents as dynamical (i.e., moving) particles. This dynamical treatment eliminates several common approximations used in other energy loss models - such as static scattering centers and vacuum-like propagators - and naturally regularizes the infrared divergences that often arise in those approaches.

2. **Unified treatment of collisional and radiative energy loss:** Both collisional [27] and radiative [28, 29] energy loss mechanisms are calculated within the same theoretical framework. Importantly:

   - For radiative energy loss, the finite size of the medium induces a nonlinear path-length dependence, interpolating between the Gunion-Bertsch limit (incoherent radiation) and the Landau-Pomeranchuk-Migdal (LPM) suppression due to coherence effects.
   - For collisional energy loss, the path-length dependence is found to be nearly linear, and finite-size corrections can safely be neglected [27].

3. **Applicability to both light and heavy flavors:** The formalism is fully applicable to partons of any mass - light quarks, charm, and bottom - allowing predictions across a broad set of experimental observables.

4. **Direct dependence on medium temperature:** Temperature T naturally enters the formalism as a dynamical quantity [30]. This enables direct input of temperature profiles from hydrodynamic or transport models of the QGP.

In other words, the formalism can be embedded into full simulations of the medium evolution.

5. **Non-perturbative QCD effects:** The formalism includes non-perturbative features of QCD, such as chromoelectric and chromomagnetic screening, implemented in a way that is consistent with lattice QCD results [31].

6. **No additional tuning to data:** Model predictions are obtained using standard parameter values from the literature, without further adjustment to fit high-p_T data [32, 33].

Thanks to these features, the dynamical energy loss model has successfully explained a wide variety of high-p_T observables [34, 35], including unexpected or -puzzling- results [36, 37, 38], as well as predictive studies for upcoming experimental runs [39, 40]. By reproducing such a broad set of data without parameter tuning, the model provides strong support for a realistic microscopic description of parton-medium interactions.

In comparison, many widely used models (such as [41, 42, 42, 43, 44, 45, 46, 47], or their subsequent extensions) may implement subsets of these features, but none incorporate all - or even most - of them. These combined properties establish the dynamical energy loss formalism as the state-of-the-art framework for quantitative QGP tomography.

Finally, since temperature is the only required input in the model, this opens a powerful opportunity: once the temperature profile is constrained by low-p_T observables (e.g., flow coefficients), the same profile can be tested against high-p_T data. Thus, the dynamical energy loss formalism enables a consistent and unified analysis of both low- and high-p_T regimes, ultimately leading to tighter constraints on the fundamental properties of the quark-gluon plasma.

8. *DREENA: A numerical framework for QGP tomography*

Implementation Strategy Behind the DREENA Framework

To reliably extract information about the QGP from high-$p_\perp$ observables, one requires a numerically efficient framework that satisfies several essential criteria:

- It must accept as input an *arbitrary temperature evolution* of the QGP - including fluctuating, event-by-event profiles from hydrodynamic simulations.

- It should preserve all essential theoretical ingredients of the underlying dynamical energy loss formalism, as each component plays an important role in accurately describing parton-medium interactions [48].

- The numerical implementation must remain computationally tractable, allowing for large-scale simulations across different systems and collision energies.
- It must generate predictions for a wide class of observables: high-$p_\perp$ light and heavy flavor R_{AA}, v_2, and higher harmonics, different collision energies (RHIC, LHC), and varying centralities.
- The computational procedure needs to be efficient, to be able to generate a comprehensive set of light and heavy flavor predictions, through the same numerical framework and the same parameter set. Such predictions can then be compared with the available experimental data, if needed iteratively for different combinations of QGP medium parameters, to extract medium properties that are consistent with both low and high-$p_\perp$ theory and data.

To meet these criteria, we developed the DREENA framework in successive stages. The initial version, DREENA-C [49], was based on a constant-temperature QGP, followed by DREENA-B [50], which incorporated an analytically solvable 1D Bjorken expansion. These simpler setups enabled semi-analytic control and testing of individual theoretical components, laying the foundation for the development of a more comprehensive numerical implementation.

The current version, DREENA-A [51], extends the approach to arbitrary three-dimensional temperature profiles obtained from hydrodynamic simulations, and is optimized for high-performance computation along path-dependent parton trajectories. Most recently, ebeDREENA [52] introduced support for full event-by-event medium evolution, enabling systematic studies of QGP fluctuations and initial-state variability. The complete algorithm is detailed in Refs. [51, 52], and the source code is publicly available [53]. The theoretical foundations and key ingredients behind the framework are summarized in the following section.

9. *Overview of the framework development*

9.1. Parton evolution in a QGP: From production to fragmentation

In high-energy heavy-ion collisions, a key goal is to understand how energetic quarks and gluons (collectively known as partons), produced in the initial hard scattering, transform into the hadrons that are eventually observed in the detector. This transformation is influenced by the presence - or absence - of QGP, a hot and dense QCD medium created in such collisions.

To quantitatively describe hadron production in the presence of a QGP, we start from a factorized expression that captures the three main stages of parton evolution:

1. The initial distribution of high-transverse-momentum partons, calculated using perturbative QCD;

2. The energy loss these partons experience while propagating through the QGP, if such a medium is formed;

3. The fragmentation of these partons into hadrons, which occurs after they exit the medium.

The combined effect of these stages leads to the following schematic expression for the final (quenched) hadron spectrum:

$$\frac{E_f d^3\sigma_q(H_Q)}{dp_f^3} = \frac{E_i d^3\sigma(Q)}{dp_i^3} \otimes P(E_i \to E_f) \otimes D(Q \to H_Q)\,, \tag{9.1}$$

Here, the symbol $\otimes$ denotes a generic convolution over relevant variables. The probability distribution $P(E_i \to E_f)$ encodes how the initial parton energy E_i is modified to a final energy E_f due to interactions with the QCD medium.

This process is illustrated in Fig. 1, where the correspondence between the physical stages and the components of Eq. (9.1) is made explicit.

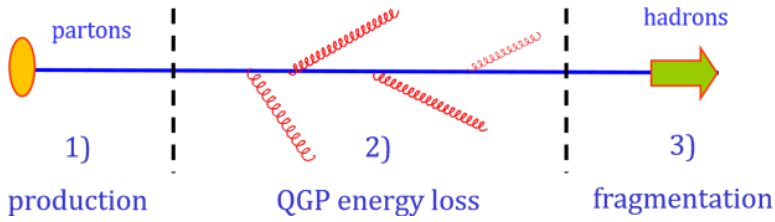

Figure 1: Schematic illustration of parton suppression in a QGP medium. The three key stages are: (1) production of high-energy partons through initial hard scattering; (2) medium-induced energy loss as the parton traverses the QGP; and (3) fragmentation into final-state hadrons after exiting the medium. These stages are treated as sequential and factorized in the theoretical calculation of the medium-modified hadron spectra, as encoded in Eq. (9.1)

In the absence of a QGP – as in proton-proton collisions – there is no medium-induced energy loss, and the expression for the final (unquenched) spectrum, denoted by u, reduces to:

$$\frac{E_f d^3\sigma_u(H_Q)}{dp_f^3} = \frac{E_i d^3\sigma(Q)}{dp_i^3} \otimes D(Q \to H_Q)\,. \tag{9.2}$$

Let us briefly define the terms involved:

- $\frac{E_f d^3\sigma_q(H_Q)}{dp_f^3}$ and $\frac{E_f d^3\sigma_u(H_Q)}{dp_f^3}$ denote the final hadron spectrum in the presence and absence of the QCD medium, respectively;

- Subscripts i and f refer to -initial- and -final-;

- Q represents the initial partons (quarks and gluons), while H_Q refers to the final hadrons formed from them;

- The initial parton spectra, $\frac{E_i d^3\sigma(Q)}{dp_i^3}$, are computed at next-to-leading order (NLO) in perturbative QCD for both light and heavy flavors [54, 55];

- $P(E_i \to E_f)$ represents the probability distribution for parton energy loss, combining radiative and collisional processes. It is computed in a realistic QCD medium - finite in size and temperature, dynamically evolving, and featuring running coupling, as well as multigluon [56] and path-length fluctuations [57];

- $D(Q \to H_Q)$ represents the fragmentation function - the probability that a parton Q fragments into a hadron H_Q with a given momentum fraction. We use DSS [58] for charged hadrons, BCFY [59] for D mesons, and KLP [60] for B mesons.

9.2. Medium evolution and collisional and radiative energy loss in DREENA–A framework

In the DREENA-A framework, one of the essential ingredients for calculating the probability of energy loss $P(E_i \to E_f)$ is the temperature of the QCD medium. Importantly, this temperature is not uniform but depends on the space-time position of the parton as it propagates through the medium. Specifically, it is determined by an externally provided temperature profile.

This means that the temperature experienced by a parton along its path becomes a function of its initial coordinates $(\mathrm{x}_0, \mathrm{y}_0)$, the angle of its trajectory ϕ, and the proper time τ along its path. This dependence is encoded by:

$$T(\mathrm{x}_0, \mathrm{y}_0, \phi, \tau) = T_{profile}(\mathrm{x}_0 + \tau\cos\phi, \mathrm{y}_0 + \tau\sin\phi, \tau), \tag{9.3}$$

where $T_{profile}$ is the local temperature of the medium, given as input and, in principle, arbitrary.

This temperature enters directly into the computation of collisional energy loss,

which is given in analytic form as [27]:

$$\frac{dE_{col}}{d\tau} = \frac{2C_R}{\pi\, v^2}\alpha_S(E\,T)\,\alpha_S(\mu_E^2(T))\int_0^\infty n_{eq}(|\vec{\mathbf{k}}|,T)d|\vec{\mathbf{k}}| \times \left(\int_0^{|\vec{\mathbf{k}}|/(1+v)} d|\vec{\mathbf{q}}|\int_{-v|\vec{\mathbf{q}}|}^{v|\vec{\mathbf{q}}|}\omega d\omega \;+\int_{|\vec{\mathbf{k}}|/(1+v)}^{|\vec{\mathbf{q}}|_{max}} d|\vec{\mathbf{q}}|\int_{|\vec{\mathbf{q}}|-2|\vec{\mathbf{k}}|}^{v|\vec{\mathbf{q}}|}\omega d\omega\right) \times \left(|\Delta_L(q,T)|^2\frac{(2|\vec{\mathbf{k}}|+\omega)^2-|\vec{\mathbf{q}}|^2}{2} + |\Delta_T(q,T)|^2\frac{(|\vec{\mathbf{q}}|^2-\omega^2)((2|\vec{\mathbf{k}}|+\omega)^2+|\vec{\mathbf{q}}|^2)}{4|\vec{\mathbf{q}}|^4}(v^2|\vec{\mathbf{q}}|^2-\omega^2)\right). \tag{9.4}$$

Let us clarify the physical meaning of each term:

- k is the four-momentum of the incoming thermal parton from the medium.
- T is the local temperature along the energetic parton path, as defined in Eq. (9.3).
- $n_{eq}(|\vec{\mathbf{k}}|,T)$ is the thermal distribution of partons in the QCD medium:

$$n_{eq}(|\vec{\mathbf{k}}|,T) = \frac{N}{e^{|\vec{\mathbf{k}}|/T}-1}+\frac{N_f}{e^{|\vec{\mathbf{k}}|/T}+1},$$

  where $N = 3$ is the number of colors, and N_f is the number of effective quark flavors ($N_f = 3$ for LHC, $N_f = 2.5$ for RHIC).
- $q = (\omega, \vec{\mathbf{q}})$ is the four-momentum of the exchanged gluon.
- $E = \sqrt{p^2+M^2}$ is the energy of the initial energetic parton (with momentum p and mass M), and $v = p/\sqrt{p^2+M^2}$ is its velocity.
- C_R is the color factor: $C_R = 4/3$ for energetic quarks and $C_R = 3$ for gluons.
- $\Delta_L(T)$ and $\Delta_T(T)$ are the longitudinal and transverse gluon propagators, respectively [25, 26].

The expression also involves the Debye mass $\mu_E(T)$, which accounts for electric screening in the QGP. This mass is determined self-consistently from [61]:

$$\frac{\mu_E(T)^2}{\Lambda_{QCD}^2}\ln\left(\frac{\mu_E(T)^2}{\Lambda_{QCD}^2}\right) = \frac{1+N_f/6}{11-2/3\,N_f}\left(\frac{4\pi T}{\Lambda_{QCD}}\right)^2. \tag{9.5}$$

This expression leads to values of $\mu_E(T)$ consistent with lattice QCD results [61, 62, 63].

Finally, we introduce running coupling [64]:

$$\alpha_S(Q^2) = \frac{4\pi}{(11 - 2/3N_f)\ln(Q^2/\Lambda^2_{QCD})}, \tag{9.6}$$

where Λ_{QCD} is the QCD scale parameter. In the case of collisional energy loss, this coupling appears in the form α_S^2, which is factorized into two scales - evaluated at $Q^2 = \mu_E^2$ and $Q^2 = E\,T$, respectively [65, 34].

This expression provides a dynamical and temperature-dependent description of energy loss due to elastic interactions, forming one of the core ingredients in the DREENA-A predictions for parton quenching in heavy-ion collisions.

In addition to collisional (elastic) interactions, partons traversing the QGP can lose energy by radiating gluons. This process is known as radiative energy loss and is typically the dominant mechanism in the high-energy regime.

In dynamical energy loss [28], the differential spectrum of radiated gluons is given by:

$$\begin{aligned}\frac{d^2N_{\rm rad}}{dxd\tau} = \int \frac{d^2k}{\pi}\,\frac{d^2q}{\pi}\,\frac{2\,C_RC_2(G)\,T}{x}\,\frac{\mu_E(T)^2 - \mu_M(T)^2}{(\boldsymbol{q}^2+\mu_M(T)^2)(\boldsymbol{q}^2+\mu_E(T)^2)} \\ \times \frac{\alpha_S(E\,T)\,\alpha_S(\frac{\boldsymbol{k}^2+\chi(T)}{x})}{\pi}\,\frac{(\boldsymbol{k}+\boldsymbol{q})}{(\boldsymbol{k}+\boldsymbol{q})^2+\chi(T)}\left(1-\cos\left(\frac{(\boldsymbol{k}+\boldsymbol{q})^2+\chi(T)}{x(E+p_z)}\,\tau\right)\right) \\ \times\left(\frac{(\boldsymbol{k}+\boldsymbol{q})}{(\boldsymbol{k}+\boldsymbol{q})^2+\chi(T)} - \frac{\boldsymbol{k}}{\boldsymbol{k}^2+\chi(T)}\right),\end{aligned} \tag{9.7}$$

where

- $C_2(G) = 3$ is the Casimir for gluons, and C_R is the color factor of the radiating parton.
- x is the fraction of the energetic parton's longitudinal momentum carried away by the emitted gluon.
- $\boldsymbol{q}$ and $\boldsymbol{k}$ are the transverse momenta of the exchanged (virtual) and radiated gluon, respectively.
- p_z is the longitudinal component of the initial energetic parton momentum, and τ is the proper time along the parton trajectory.
- The function $\chi(T)$ is defined as:

$$\chi(T) \equiv M^2x^2 + m_g(T)^2,$$

where M is the energetic parton mass, and $m_g(T) = \mu_E(T)/\sqrt{2}$ is the effective gluon mass in a thermal QCD medium [66].

- For charm quarks we take $M = 1.3$ GeV, and for bottom $M = 4.5$ GeV [55]; for light quarks, the effective mass is taken as $\mu_E(T)/\sqrt{6}$, originating from gluon propagators.

- $\mu_E(T)$ is the Debye mass, as previously defined, and $\mu_M(T)$ represents the magnetic screening mass. Lattice-inspired non-perturbative studies suggest (cf. [62, 63])
$$0.4 < \mu_M(T)/\mu_E(T) < 0.6.$$

- The running coupling α_S appears in two scales:
$$\alpha_S(ET) \quad \text{and} \quad \alpha_S\left(\frac{\boldsymbol{k}^2 + \chi(T)}{x}\right),$$
where the second scale corresponds to the virtuality of the radiating parton prior to gluon emission [28].

An important feature of this formulation is that all terms involving α_S are infrared safe – they remain finite even at low momentum transfers - and take moderate values throughout the integration domain [34]. As a result, we do not need to introduce an artificial cutoff in the strong coupling, which distinguishes this approach from many others in the literature.

Treatment of combined energy loss mechanisms.

In our model, we treat radiative and collisional energy losses as two independent stochastic processes, each contributing to the overall energy loss probability $P(E_i \to E_f)$ [34, 57]. This means that we:

1. First calculate the modification of the parton spectrum due to radiative energy loss.

2. Then apply the effect of collisional energy loss on the radiatively modified spectrum.

We have verified that changing the order of these two steps does not significantly alter the result, within the precision of our framework.

This treatment is justified under the assumptions that:

- Both energy loss mechanisms are relatively small, consistent with the soft-gluon and soft-rescattering approximations commonly used in energy loss physics.

- The two processes are decoupled - as is the case in the generalized Hard Thermal Loop (HTL) framework [28], which underlies our calculation.

This modular approach allows us to isolate the physics of each mechanism while still capturing their combined effect on high-momentum parton propagation through the QGP.

To incorporate both energy loss mechanisms into a single probability distribution $P(E_i \to E_f)$, we treat radiative and collisional processes as independent stochastic events. The total probability is constructed by convolving their respective distributions - a Poisson distribution for radiative loss and a Gaussian for collisional fluctuations - and is subsequently used to compute the medium-modified hadron spectrum.

Hadron suppression observables.

The nuclear modification factor $R^{tr}_{AA}(p_f, H_Q)$ for a single trajectory is defined as the ratio of quenched to unquenched hadron spectra:

$$R^{tr}_{AA}(p_f, H_Q) = \frac{E_f d^3\sigma_q(H_Q)}{dp_f^3} \Bigg/ \frac{E_f d^3\sigma_u(H_Q)}{dp_f^3}, \tag{9.8}$$

where the unquenched spectrum is given by Eq. (9.2).

To account for azimuthal variations, we average over all trajectories with a fixed direction angle ϕ, yielding the angle-dependent suppression:

$$R_{AA}(p_f, \phi, H_Q) = \langle R^{tr}_{AA}(p_f, H_Q)\rangle_{\text{trajectories at angle } \phi}.$$

This step is essential: due to spatial asymmetries and gradients in the QGP temperature profile, energy loss depends not only on the path length but also on the direction of propagation.

Finally, we compute the standard observables $R_{AA}(p_\perp)$ and $v_2(p_\perp)$ as:

$$R_{AA}(p_\perp) = \frac{1}{2\pi}\int_0^{2\pi} R_{AA}(p_\perp, \phi)d\phi, \tag{9.9}$$

and

$$v_2(p_\perp) = \frac{\dfrac{1}{2\pi}\displaystyle\int_0^{2\pi} \cos(2\phi) R_{AA}(p_\perp, \phi)d\phi}{R_{AA}(p_\perp)}, \tag{9.10}$$

respectively. Here we omit the hadron label H_Q for clarity, and denote $p_f = p_\perp$.

9.3. Testing sensitivity of high-$p_\perp$ probes to QGP evolution

Once we constructed a numerical framework capable of simulating parton energy loss in an arbitrarily evolving QGP medium, a fundamental question arises: *can*

high-$p_\perp$ observables meaningfully differentiate between different temperature evolution scenarios? In other words, do these probes possess sufficient sensitivity to provide additional constraints on the QGP evolution beyond those already imposed by low-$p_\perp$ bulk observables?

To explore this, we selected three widely used medium evolution models

– OptGlauber+3D hydro [67],

– EKRT+3D hydro [67, 68], and

–TRENTo+VISHNU [69, 70],

all of which reproduce soft-sector observables (e.g., multiplicity distributions and collective flow harmonics). However, despite this agreement at low transverse momenta, their corresponding temperature profiles differ significantly, both in geometry and magnitude.

Figure 2 illustrates these differences by comparing the temperature distributions in the transverse plane at different time slices, $\tau = \tau_0$, 2, 3, 4, and 5 fm/c, for 30-40% central Pb+Pb collisions at $\sqrt{s_{NN}} = 5.02$ TeV. The OptGlauber profile exhibits the most pronounced spatial anisotropy, suggesting it may yield the largest azimuthal anisotropy v_2 for high-$p_\perp$ hadrons. In contrast, the TRENTo+VISHNU setup produces a nearly isotropic temperature distribution, which is expected to result in a small v_2. Meanwhile, EKRT evolution achieves the highest initial temperatures, indicating it may lead to the strongest parton energy loss and, consequently, the smallest nuclear modification factor R_{AA}.

To determine whether these qualitative differences in temperature evolution affect high-$p_\perp$ observables, we used the DREENA-A framework to compute R_{AA} and v_2 for charged hadrons, D, and B mesons at the LHC, using each of the three hydrodynamic models described above.

The results, presented in Figure 3, show clear correlations between the temperature evolution and the predicted observable values:

- The EKRT-based profile, with the highest temperatures, produces the strongest suppression - i.e., the lowest R_{AA} values - as expected due to enhanced energy loss.
- The OptGlauber evolution, with the largest spatial anisotropy, yields the highest v_2.
- The more isotropic TRENTo profile leads to the smallest elliptic flow.

These findings confirm that high-$p_\perp$ observables are indeed sensitive to QGP temperature evolution and can be used to discriminate among different hydrodynamic models. In combination with a robust theoretical framework, this sensitivity establishes high-$p_\perp$ probes as a valuable tool for QGP tomography.

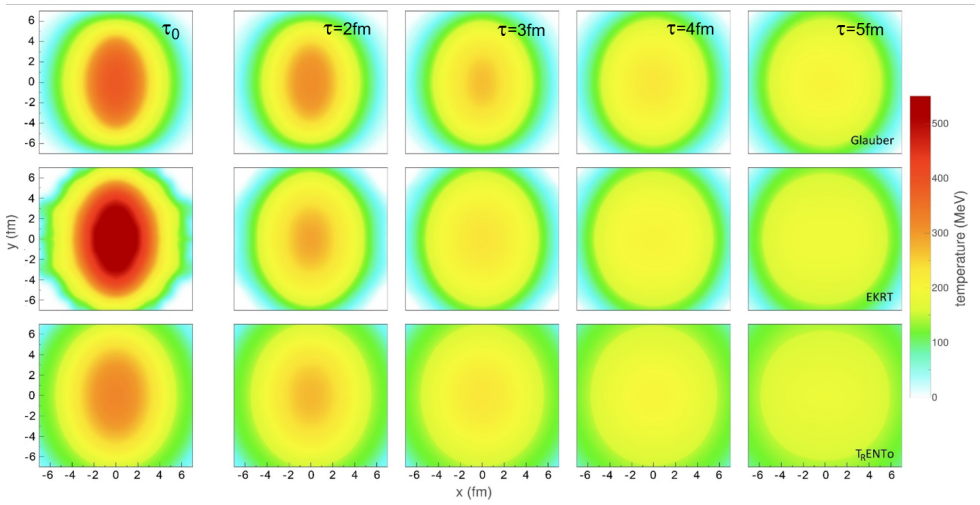

Figure 2: Temperature evolution for 30-40% central Pb+Pb collisions at $\sqrt{s_{NN}} = 5.02$ TeV, obtained from three hydrodynamic models: OptGlauber+3D Hydro (top row), EKRT+3D Hydro (middle row), and TRENTo+VISHNU (bottom row). Each column corresponds to a different proper time: $\tau = \tau_0, 2, 3, 4, 5$ fm/c (left to right). Note that the initial times τ_0 differ among the models. Figure from [51]

9.4. From observables to tomography

The primary aim of this review was to provide the outline of the development of a physically consistent and numerically efficient framework - based on the dynamical energy loss formalism - capable of describing high-$p_\perp$ parton–medium interactions in a finite, evolving QCD medium. Building on this foundation, the DREENA framework was created to enable systematic comparisons between theoretical predictions and experimental data across a broad range of observables and energies.

Developed within an ERC Consolidator project focused on QGP tomography, this research program has led to a series of analyses that demonstrate the utility of high-$p_\perp$ observables as precision tools for probing the QGP. Below we summarize key results that illustrate the power of the DREENA framework in extracting information about the QGP properties:

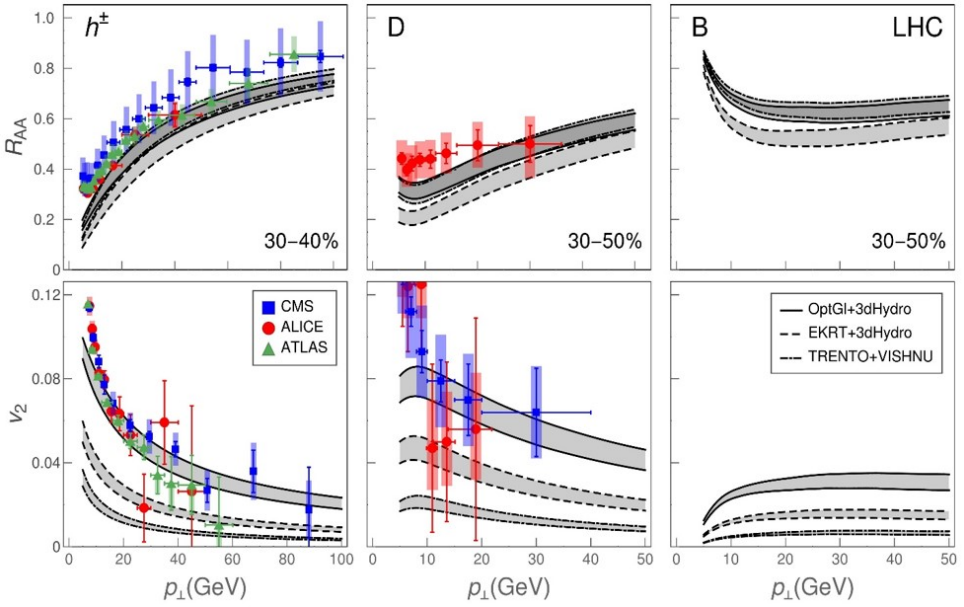

Figure 3: DREENA-A predictions for R_{AA} (top row) and v_2 (bottom row) for charged hadrons, D, and B mesons in 30-40% central Pb+Pb collisions at $\sqrt{s_{NN}} = 5.02$ TeV. Theoretical predictions are shown for three different temperature profiles: OptGlauber+3D Hydro (solid line), EKRT+3D Hydro (dashed), and TRENTo+VISHNU (dot-dashed). Data points are from ALICE, ATLAS, and CMS [71, 72, 73, 74, 75, 76, 77, 78, 79]. Figure from [51]

- **Constraining the early-time QGP evolution.** A central open question in heavy-ion physics is how the quark-gluon plasma behaves during the earliest moments after the collision - before it reaches thermal equilibrium. Using high-$p_\perp$ observables as tomographic probes, we examined the sensitivity of R_{AA} and v_2 to the earliest stages of medium evolution. Employing the DREENA-A framework coupled with 3+1D hydrodynamic backgrounds, we found that the data systematically favor a delayed onset of energy loss and transverse expansion. In particular, heavy-flavor observables exhibit a pronounced sensitivity to these early-time dynamics. These results demonstrate, for the first time, that the bulk evolution of the QGP - traditionally constrained by soft-sector observables - can also be independently constrained through high-p_T quenching phenomena [32].

- **Connecting energy loss to shear viscosity.** We analytically derived the temperature dependence of the shear viscosity to entropy density ratio, $\eta/s(T)$, from the dynamical energy loss formalism. The resulting profile shows strik-

ing agreement with hydrodynamically extracted $\eta/s(T)$ from low-$p_\perp$ Bayesian analyses - including near T_c, where strong coupling effects dominate. This provides an independent, theory-based constraint on η/s, which way support the quasiparticle picture of QGP [83].

- **Jet-perceived anisotropy.** We introduced the concept of *average jet-temperature anisotropy* as a medium property directly experienced by high-energy partons. Using DREENA-A simulations, we showed that the ratio $v_2/(1-R_{AA})$ saturates to a value proportional to this anisotropy, enabling its extraction from experimental data. This provides a novel constraint on medium evolution models and represents one of the first direct, data-driven probes of intrinsic QGP geometry using high-$p_\perp$ observables [33].

- **Event-by-event tomography.** To explore the fluctuating geometry of the QGP, we extended the DREENA-A framework to fully event-by-event simulations. This extension enabled us to demonstrate that higher-order flow harmonics (v_3, v_4) are sensitive to the fluctuating initial conditions of the medium, and that different initialization models lead to distinct predictions. Notably, none of the currently available hydrodynamic profiles can reproduce the measured v_4 at high $p_\perp$, suggesting a potential tension - the so-called v_4 *puzzle* - between theory and data [52].

  Additionally, within the same event-by-event framework, we used high-$p_\perp$ observables to constrain the QGP-s initial geometry and early-time evolution, highlighting the power of QGP tomography to probe the medium's earliest stages [84].

Together, these results underscore the versatility and predictive power of the DREENA framework. More broadly, they show that high-$p_\perp$ observables - when analyzed within a realistic and systematically improvable theoretical formalism - can serve as precision tools for extracting properties of the QCD medium.

10. *Conclusion*

In this work, we have integrated two traditionally distinct domains of heavy-ion physics - high-energy parton energy loss and relativistic hydrodynamics - into a unified, dynamically consistent framework. This integration led to the development of DREENA: a versatile numerical tool designed to simulate high-$p_\perp$ parton-medium interactions within a realistic QGP background and to systematically compare theoretical predictions with hadron experimental data across a wide range of collision systems, centralities, probes, and energies.

The resulting framework has enabled quantitative studies of essential QGP properties – such as temperature evolution, viscosity, and thermalization time – by jointly

analyzing complementary sets of low- and high-$p_\perp$ observables. Of particular significance is the fact that these diverse measurements, traditionally studied separately, can now be combined to provide consistent constraints on the medium-s global features.

Although this approach involved a substantial theoretical challenge, the outcome has been highly rewarding: it allowed us to repurpose the wealth of high-$p_\perp$ data collected at RHIC and the LHC into an active probe of QGP properties. This expands the role of high-$p_\perp$ measurements from merely testing energy-loss models to serving as precision tools for QGP tomography.

Looking ahead, the DREENA framework establishes the theoretical framework necessary for the upcoming precision era in heavy-ion physics. With the expected increase in experimental accuracy during LHC Run 3 and at sPHENIX, DREENA is well-positioned to deliver robust quantitative constraints of QGP parameters, thus maximizing the scientific return from major collider investments and pushing the field toward a new level of quantitative understanding.

Acknowledgements: MD acknowledges support from the European Research Council (ERC Consolidator Grant No. 725741), the Ministry of Science and Technological Development of the Republic of Serbia, and the Serbian Academy of Sciences and Arts.

REFERENCES

[1] J. C. Collins and M. J. Perry, *Superdense matter: neutrons or asymptotically free quarks?*, Phys. Rev. Lett. **34** (1975), 1353–1356.

[2] G. Baym and S. A. Chin, *Can a neutron star be a giant MIT bag?*, Phys. Lett. B **62** (1976), 241–244.

[3] E. V. Shuryak, *What RHIC experiments and theory tell us about properties of quark-gluon plasma?*, Nucl. Phys. A **750** (2005), 64–83; E. Shuryak, *Strongly coupled quark-gluon plasma in heavy ion collisions*, Rev. Mod. Phys. **89** (2017), Article 035001.

[4] M. Gyulassy and L. McLerran, *New forms of QCD matter discovered at RHIC*, Nucl. Phys. A **750** (2005), 30–63.

[5] B. Jacak and P. Steinberg, *Creating the perfect liquid in heavy-ion collisions*, Phys. Today **63**(5) (2010), 39–43.

[6] B. Muller, J. Schukraft and B. Wyslouch, *First results from Pb+Pb collisions at the LHC*, Annu. Rev. Nucl. Part. Sci. **62** (2012), 361–386.

[7] R. Stock, *The physics of dense nuclear matter from supernovae to quark-gluon plasma*, Nature **337** (1989), 319–324.

[8] J. Stachel, *Has the quark-gluon plasma been seen?*, Int. J. Mod. Phys. A **21** (2006), 1750–1763.

[9] U. Heinz and R. Snellings, *Collective flow and viscosity in relativistic heavy-ion collisions*, Annu. Rev. Nucl. Part. Sci. **63** (2013), 123–151.

[10] J. D. Bjorken, *Energy loss of energetic partons in quark-gluon plasma: Possible extinction of high p_T jets in hadron-hadron collisions*, Fermilab Report No. FERMILAB-Pub-82/59-THY (1982).

[11] B. V. Jacak and B. Muller, *The exploration of hot nuclear matter*, Science **337** (2012), 310–314.

[12] P. Kovtun, D. T. Son and A. O. Starinets, *Viscosity in strongly interacting quantum field theories from black hole physics*, Phys. Rev. Lett. **94** (2005), Article 111601.

[13] C. V. Johnson and P. Steinberg, *What black holes teach about strongly coupled particles*, Phys. Today **63**(5) (2010), 29–33.

[14] H. Niemi, G. S. Denicol, P. Huovinen, E. Molnar and D. H. Rischke, *Influence of shear viscosity of quark-gluon plasma on elliptic flow in ultrarelativistic heavy-ion collisions*, Phys. Rev. Lett. **106** (2011), Article 212302.

[15] J. L. Nagle, I. G. Bearden and W. A. Zajc, *Quark-gluon plasma at the RHIC and the LHC: perfect fluid too perfect?*, New J. Phys. **13** (2011), Article 075004.

[16] J. Auvinen, K. J. Eskola, P. Huovinen, H. Niemi, R. Paatelainen and P. Petreczky, *Temperature dependence of η/s of strongly interacting matter: Effects of the equation of state and the parametric form of $(\eta/s)(T)$*, Phys. Rev. C **102** (2020), Article 044911.

[17] J. D. Orjuela Koop, A. Adare, D. McGlinchey and J. L. Nagle, *Azimuthal anisotropy relative to the participant plane from a multiphase transport model in central p+Au, d+Au, and ^{3}He+Au collisions at $\sqrt{s_{NN}} = 200$ GeV*, Phys. Rev. C **92** (2015), Article 054903.

[18] J. Auvinen, J. E. Bernhard, S. A. Bass and I. Karpenko, *Investigating the collision energy dependence of η/s in the beam energy scan at the BNL Relativistic Heavy Ion Collider using Bayesian statistics*, Phys. Rev. C **97** (2018), Article 044905.

[19] L. P. Csernai, J. I. Kapusta and L. D. McLerran, *Strongly interacting low-viscosity matter created in relativistic nuclear collisions*, Phys. Rev. Lett. **97** (2006), Article 152303.

[20] J. E. Bernhard, J. S. Moreland and S. A. Bass, *Bayesian estimation of the specific shear and bulk viscosity of quark-gluon plasma*, Nature Phys. **15** (2019), 1113–1117.

[21] D. Everett *et al.* [JETSCAPE Collaboration], *Multisystem Bayesian constraints on the transport coefficients of QCD matter*, Phys. Rev. C **103** (2021), Article 054904.

[22] G. Nijs and W. van der Schee, *Hadronic nucleus-nucleus cross section and the nucleon size*, Phys. Rev. Lett. **129** (2022), Article 232301.

[23] M. R. Heffernan, C. Gale, S. Jeon and J.-F. Paquet, *Bayesian quantification of strongly interacting matter with color glass condensate initial conditions*, Phys. Rev. C **109** (2024), Article 065207.

[24] D. Molnar and D. Sun, *Interplay between bulk medium evolution and (D)GLV energy loss*, Nucl. Phys. A **932** (2014), 140–145; D. Molnar and D. Sun, *Realistic medium-averaging in radiative energy loss*, Nucl. Phys. A **910-911** (2013), 486–489.

[25] J. I. Kapusta, *Finite-Temperature Field Theory* (Cambridge University Press, Cambridge, 1989).

[26] M. Le Bellac, *Thermal Field Theory* (Cambridge University Press, Cambridge, 1996).

[27] M. Djordjevic, *Collisional energy loss in a finite size QCD medium*, Phys. Rev. C **74** (2006), Article 064907.

[28] M. Djordjevic, *Theoretical formalism of radiative jet energy loss in a finite size dynamical QCD medium*, Phys. Rev. C **80** (2009), Article 064909.

[29] M. Djordjevic and U. Heinz, *Radiative energy loss in a finite dynamical QCD medium*, Phys. Rev. Lett. **101** (2008), Article 022302.

[30] S. Stojku, B. Ilic, M. Djordjevic and M. Djordjevic, *Extracting the temperature dependence in high-p_T particle energy loss*, Phys. Rev. C **103** (2021), Article 024908.

[31] M. Djordjevic and M. Djordjevic, *Generalization of radiative jet energy loss to non-zero magnetic mass*, Phys. Lett. B **709** (2012), 229–233.

[32] S. Stojku, J. Auvinen, M. Djordjevic, P. Huovinen and M. Djordjevic, *Early evolution constrained by high-p_T quark-gluon plasma tomography*, Phys. Rev. C **105** (2022), Article L021901.

[33] S. Stojku, J. Auvinen, L. Zivkovic, P. Huovinen and M. Djordjevic, *Jet-perceived anisotropy revealed through high-$p_\perp$ data*, Phys. Lett. B **835** (2022), Article 137501.

[34] M. Djordjevic and M. Djordjevic, *LHC jet suppression of light and heavy flavor observables*, Phys. Lett. B **734** (2014), 286–289.

[35] M. Djordjevic, M. Djordjevic and B. Blagojevic, *RHIC and LHC jet suppression in non-central collisions*, Phys. Lett. B **737** (2014), 298–302.

[36] M. Djordjevic, *Heavy flavor puzzle at LHC: A serendipitous interplay of jet suppression and fragmentation*, Phys. Rev. Lett. **112** (2014), Article 042302.

[37] M. Djordjevic and M. Djordjevic, *Heavy flavor puzzle from data measured at the BNL Relativistic Heavy Ion Collider: Analysis of the underlying effects*, Phys. Rev. C **90** (2014), Article 034910.

[38] M. Djordjevic and M. Djordjevic, *Understanding the unexpected suppression patterns at RHIC and LHC*, Mod. Phys. Lett. A **29** (2014), Article 1430035.

[39] M. Djordjevic and M. Djordjevic, *Predictions of heavy-flavor suppression at 5.1 TeV Pb+Pb collisions at the CERN Large Hadron Collider*, Phys. Rev. C **92** (2015), Article 024918.

[40] M. Djordjevic, *Complex suppression patterns distinguish between major energy loss effects in quark-gluon plasma*, Phys. Lett. B **763** (2016), 439–444.

[41] R. Baier, Yu. L. Dokshitzer, A. H. Mueller, S. Peigne and D. Schiff, *Radiative energy loss and p_T-broadening of high-energy partons in nuclei*, Nucl. Phys. B **484** (1997), 265–282.

[42] B. G. Zakharov, *Fully quantum treatment of the Landau-Pomeranchuk-Migdal effect in QED and QCD*, JETP Lett. **63** (1996), 952–957; B. G. Zakharov, *Radiative energy loss of high-energy quarks in finite-size nuclear matter and quark-gluon plasma*, JETP Lett. **65** (1997), 615–620.

[43] N. Armesto, C. A. Salgado and U. A. Wiedemann, *Medium-induced gluon radiation off massive quarks fills the dead cone*, Phys. Rev. D **69** (2004), Article 114003.

[44] M. Gyulassy, P. Levai and I. Vitev, *Reaction operator approach to non-Abelian energy loss*, Nucl. Phys. B **594** (2001), 371–419.

[45] P. Arnold, G. D. Moore and L. G. Yaffe, *Photon emission from ultrarelativistic plasmas*, JHEP **11** (2001), Article 057; P. Arnold, G. D. Moore and L. G. Yaffe, *Photon emission from quark-gluon plasma: Complete leading order results*, JHEP **12** (2001), Article 009.

[46] X.-N. Wang and X.-f. Guo, *Multiple parton scattering in nuclei: Parton energy loss*, Nucl. Phys. A **696** (2001), 788–832.

[47] A. Majumder and M. van Leeuwen, *The theory and phenomenology of perturbative QCD based jet quenching*, Prog. Part. Nucl. Phys. **66** (2011), 41–92.

[48] B. Blagojevic and M. Djordjevic, *Importance of different energy loss effects in jet suppression at RHIC and LHC*, J. Phys. G **42** (2015), Article 075105.

[49] D. Zigic, I. Salom, J. Auvinen, M. Djordjevic and M. Djordjevic, *DREENA-C framework: joint R_{AA} and v_2 predictions and implications to QGP tomography*, J. Phys. G **46** (2019), Article 085101.

[50] D. Zigic, I. Salom, J. Auvinen, M. Djordjevic and M. Djordjevic, *DREENA-B framework: First predictions of R_{AA} and v_2 within dynamical energy loss formalism in evolving QCD medium*, Phys. Lett. B **791** (2019), 236–241.

[51] D. Zigic, I. Salom, J. Auvinen, P. Huovinen and M. Djordjevic, *DREENA-A framework as a QGP tomography tool*, Front. Phys. **10** (2022), Article 957019.

[52] D. Zigic, J. Auvinen, I. Salom, M. Djordjevic and P. Huovinen, *Importance of higher harmonics and v_4 puzzle in quark-gluon plasma tomography*, Phys. Rev. C **106** (2022), Article 044909.

[53] *DREENA-A*, GitHub repository, `https://github.com/DusanZigic/DREENA-A`.

[54] Z.-B. Kang, I. Vitev and H. Xing, *Nuclear modification of high transverse momentum particle production in p+A collisions at RHIC and LHC*, Phys. Lett. B **718** (2012), 482–487; R. Sharma, I. Vitev and B.-W. Zhang, *Light-cone wave function approach to open heavy flavor dynamics in QCD matter*, Phys. Rev. C **80** (2009), Article 054902.

[55] M. Cacciari, S. Frixione, N. Houdeau, M. L. Mangano, P. Nason and G. Ridolfi, *Theoretical predictions for charm and bottom production at the LHC*, JHEP **10** (2012), Article 137.

[56] M. Gyulassy, P. Levai and I. Vitev, *Jet tomography of Au+Au reactions including multigluon fluctuations*, Phys. Lett. B **538** (2002), 282–288.

[57] S. Wicks, W. Horowitz, M. Djordjevic and M. Gyulassy, *Elastic, inelastic, and path length fluctuations in jet tomography*, Nucl. Phys. A **784** (2007), 426–442.

[58] D. de Florian, R. Sassot and M. Stratmann, *Global analysis of fragmentation functions for pions and kaons and their uncertainties*, Phys. Rev. D **75** (2007), Article 114010.

[59] M. Cacciari and P. Nason, *Charm cross sections for the Tevatron Run II*, JHEP **09** (2003), Article 006; E. Braaten, K.-m. Cheung, S. Fleming and T. C. Yuan, *Perturbative QCD fragmentation functions as a model for heavy quark fragmentation*, Phys. Rev. D **51** (1995), 4819–4829.

[60] V. G. Kartvelishvili, A. K. Likhoded and V. A. Petrov, *On the fragmentation functions of heavy quarks into hadrons*, Phys. Lett. B **78** (1978), 615–617.

[61] A. Peshier, *Running coupling and screening in the (s)QGP*, `arXiv:hep-ph/0601119` (2006).

[62] Yu. Maezawa *et al.* [WHOT-QCD Collaboration], *Electric and magnetic screening masses at finite temperature from generalized Polyakov-line correlations in two-flavor lattice QCD*, Phys. Rev. D **81** (2010), Article 091501(R).

[63] A. Nakamura, T. Saito and S. Sakai, *Lattice calculation of gluon screening masses*, Phys. Rev. D **69** (2004), Article 014506.

[64] R. D. Field, *Applications of Perturbative QCD* (Perseus Books, Cambridge, MA, 1995).

[65] S. Peigne and A. Peshier, *Collisional energy loss of a fast heavy quark in a quark-gluon plasma*, Phys. Rev. D **77** (2008), Article 114017.

[66] M. Djordjevic and M. Gyulassy, *Ter-Mikayelian effect on QCD radiative energy loss*, Phys. Rev. C **68** (2003), Article 034914.

[67] E. Molnar, H. Holopainen, P. Huovinen and H. Niemi, *Influence of temperature-dependent shear viscosity on elliptic flow at backward and forward rapidities in ultrarelativistic heavy-ion collisions*, Phys. Rev. C **90** (2014), Article 044904.

[68] K. J. Eskola, K. Kajantie, P. V. Ruuskanen and K. Tuominen, *Scaling of transverse energies and multiplicities with atomic number and energy in ultrarelativistic nuclear collisions*, Nucl. Phys. B **570** (2000), 379–389.

[69] J. S. Moreland, J. E. Bernhard and S. A. Bass, *Alternative ansatz to wounded nucleon and binary collision scaling in high-energy nuclear collisions*, Phys. Rev. C **92** (2015), Article 011901 (R).

[70] H. Song and U. W. Heinz, *Causal viscous hydrodynamics in 2+1 dimensions for relativistic heavy-ion collisions*, Phys. Rev. C **77** (2008), Article 064901.

[71] S. Acharya *et al.* [ALICE], *Transverse momentum spectra and nuclear modification factors of charged particles in pp, p-Pb and Pb-Pb collisions at the LHC*, JHEP **11** (2018), Article 013.

[72] S. Acharya *et al.* [ALICE], *Energy dependence and fluctuations of anisotropic flow in Pb-Pb collisions at* $\sqrt{s_{NN}} = 5.02$ *and 2.76 TeV*, JHEP **07** (2018), Article 103.

[73] S. Acharya *et al.* [ALICE], *Measurement of* D^0*,* D^+*,* D^{*+} *and* D_s^+ *production in Pb-Pb collisions at* $\sqrt{s_{NN}} = 5.02$ *TeV*, JHEP **10** (2018), Article 174.

[74] S. Acharya *et al.* [ALICE], *D-meson azimuthal anisotropy in mid-central Pb-Pb collisions at* $\sqrt{s_{NN}} = 5.02$ *TeV*, Phys. Rev. Lett. **120** (2018), Article 102301.

[75] [ATLAS Collaboration], *Measurement of the nuclear modification factor* R_{AA} *in Pb+Pb collisions at* $\sqrt{s_{NN}} = 5.02$ *TeV with the ATLAS detector at the LHC*, ATLAS-CONF-2017-012 (2017).

[76] M. Aaboud *et al.* [ATLAS], *Measurement of the azimuthal anisotropy of charged particles produced in* $\sqrt{s_{NN}} = 5.02$ *TeV Pb+Pb collisions with the ATLAS detector*, Eur. Phys. J. C **78** (2018), Article 997.

[77] V. Khachatryan *et al.* [CMS], *Charged-particle nuclear modification factors in PbPb and pPb collisions at* $\sqrt{s_{NN}} = 5.02$ *TeV*, JHEP **04** (2017), Article 039.

[78] A. M. Sirunyan *et al.* [CMS], *Azimuthal anisotropy of charged particles with transverse momentum up to 100 GeV in PbPb collisions at* $\sqrt{s_{NN}} = 5.02$ *TeV*, Phys. Lett. B **776** (2018), 195–216.

[79] A. M. Sirunyan *et al.* [CMS], *Measurement of prompt* D^0 *meson azimuthal anisotropy in PbPb collisions at* $\sqrt{s_{NN}} = 5.02$ *TeV*, Phys. Rev. Lett. **120** (2018), Article 202301.

[80] [sPHENIX], *sPHENIX Beam Use Proposal* (2021), https://indico.bnl.gov/event/11884/attachments/34524/56472/sPHENIX_BUP_2021.pdf.

[81] [STAR], *The STAR Beam Use Request for Run-22 and data taking in 2023–25* (2021), https://drupal.star.bnl.gov/STAR/files/STAR_Beam_Use_Request_Runs22_25.pdf.

[82] S. Fartoukh *et al.*, *LHC Configuration and Operational Scenario for Run 3*, CERN-ACC-2021-0007 (2021).

[83] B. Karmakar, D. Zigic, I. Salom, J. Auvinen, P. Huovinen, M. Djordjevic and M. Djordjevic, *Constraining η/s through high-$p_\perp$ theory and data*, Phys. Rev. C **108** (2023), Article 044907.

[84] B. Karmakar, D. Zigic, M. Djordjevic, P. Huovinen, M. Djordjevic and J. Auvinen, *Probing the shape of the quark-gluon plasma droplet via event-by-event quark-gluon plasma tomography*, Phys. Rev. C **110** (2024), Article 044906.

Institute of Physics Belgrade
University of Belgrade
Serbia
e-mail: magda@ipb.ac.rs